

# PCCP

Accepted Manuscript



This is an *Accepted Manuscript*, which has been through the Royal Society of Chemistry peer review process and has been accepted for publication.

*Accepted Manuscripts* are published online shortly after acceptance, before technical editing, formatting and proof reading. Using this free service, authors can make their results available to the community, in citable form, before we publish the edited article. We will replace this *Accepted Manuscript* with the edited and formatted *Advance Article* as soon as it is available.

You can find more information about *Accepted Manuscripts* in the [Information for Authors](#).

Please note that technical editing may introduce minor changes to the text and/or graphics, which may alter content. The journal's standard [Terms & Conditions](#) and the [Ethical guidelines](#) still apply. In no event shall the Royal Society of Chemistry be held responsible for any errors or omissions in this *Accepted Manuscript* or any consequences arising from the use of any information it contains.

**Investigation of Electron Density Changes at the  
Onset of a Chemical Reaction using the State-Specific  
Dual Descriptor from Conceptual Density Functional  
Theory**

Frank De Proft,<sup>1\*</sup> Valérian Forquet,<sup>2</sup> Benjamin Ourri,<sup>2</sup> Henry Chermette<sup>2</sup>, Paul  
Geerlings<sup>1</sup> and Christophe Morell<sup>2\*</sup>

<sup>1</sup>Research group of General Chemistry, Vrije Universiteit Brussel (VUB), Pleinlaan 2,  
B-1050 Brussels, Belgium.

<sup>2</sup>Team Chemometry and Modelling (CHEMOD), University Claude Bernard Lyon 1,  
5 Rue de la Doua, F-69100 Villeurbanne, France

**Abstract**

The electron density change from reactants towards the transition state of a chemical reaction is expressed as a linear combination of the state-specific dual descriptors (SSDD) of the corresponding reactant complexes. Consequently, the SSDD can be expected to bear important resemblance to the so-called Natural Orbitals for Chemical Valence (NOCV), introduced as the orbitals that diagonalize the deformation density matrix of interacting molecules. This agreement is shown for three case studies: the complexation of a Lewis acid with a Lewis base, a  $S_N2$  nucleophilic substitution reaction and a Diels-Alder cycloaddition reaction. As such, the SSDD computed for reactant complexes are shown to provide important information about charge transfer interactions during a chemical reaction.

## Introduction

Conceptual Density Functional Theory (also known as DFT based reactivity theory or chemical DFT) is an important tool to study problems in chemical reactivity<sup>1,2,3</sup>. In this theory, reactivity indices are introduced as response properties, *i.e.* derivatives of the energy  $E$  with respect to the number of electrons  $N$  and the external potential  $v(\mathbf{r})$ <sup>4</sup>, the two quantities of a molecule that are perturbed when it undergoes a chemical reaction. These properties can then be linked to interesting chemical quantities of which many were already known by chemists but only defined in an empirical way. Examples of these quantities include the electronegativity<sup>5-7</sup> and the concepts of hardness<sup>8-10</sup> and softness<sup>11</sup>. Other important quantities that have been introduced and enable the study of problems in regioselectivity are the Fukui function and the dual descriptor<sup>12-16</sup>. In addition, in the course of the development of the theory, other reactivity indices, such as e.g. electrophilicity<sup>17,18,19</sup> and local softness<sup>20,21</sup>, have been introduced that are not necessarily derivatives of the energy. Also, the theory has provided a framework for the rationalization and use of a number of chemical principles, such as Sanderson's principle of electronegativity equalization<sup>22,23</sup> and Pearson's Hard and Soft Acids and Bases<sup>24-28</sup> and Maximum Hardness Principles<sup>29</sup>.

It is well known that density functional theory uses the electron density  $\rho(\mathbf{r})$  of the system as the basic variable instead of the wavefunction  $\Psi$ . This is formally based on the Hohenberg-Kohn theorems<sup>30</sup> and implies that the electron density determines all ground state atomic and molecular properties. Since a chemical reaction involves the transition of a system from one ground state to another, it can ultimately be considered as a reshuffling<sup>31</sup> of the electron densities between the interacting molecules. In this contribution, we will investigate electron density changes during

the chemical reaction when going from the reactants to the transition state within a conceptual DFT framework using the recently introduced state specific dual descriptor<sup>32,33</sup>. It will be shown that this quantity, computed for a pre-reactive complex of two interacting molecules, provides an interesting connection with the Natural Orbitals for Chemical Valence (NOCV), introduced by Michalak, Mittoraj and Ziegler<sup>34,35</sup>.

### Theoretical developments

During the course of a chemical reaction, the electron density of the reacting molecules is perturbed due to the change in the external potential and the charge transfer between the reagents<sup>36</sup>. In line with the analysis of Morell *et al.*, the electron density at the transition state of the reaction  $\rho_{TS}^{(0),ext}(\mathbf{r})$  can be extrapolated from the ground and excited state electron densities of the reagents at the onset of the reaction  $\rho_R^{(i)}(\mathbf{r})$  ( $i \geq 0$ )

$$\rho_{TS}^{(0),ext}(\mathbf{r}) = \sum_{i \geq 0} \alpha_i \rho_R^{(i)}(\mathbf{r}) \quad (1)$$

In the approach we will adopt in this paper, the reactant state is considered to be the initial complex of the reacting molecules at the beginning of the intrinsic reaction coordinate. Since indeed then the left and right hand sides of (1) should integrate to the same number of electrons, this implies that

$$\sum_{i \geq 0} \alpha_i = 1 \quad (2)$$

so that Eq. (1) can be rewritten as:

$$\rho_{TS}^{(0),ext}(\mathbf{r}) = \left(1 - \sum_{i \geq 0} \alpha_i\right) \rho_R^{(0)}(\mathbf{r}) + \sum_{i \geq 0} \alpha_i \rho_R^{(i)}(\mathbf{r}) \quad (3)$$

where  $\rho_R^{(0)}(\mathbf{r})$  is the ground state electron density of the reactant complex. Then, Eq. (3) becomes

$$\rho_{TS}^{(0),ext}(\mathbf{r}) = \rho_R^{(0)}(\mathbf{r}) + \sum_{i \geq 0} \alpha_i \left(\rho_R^{(i)}(\mathbf{r}) - \rho_R^{(0)}(\mathbf{r})\right) = \rho_R^{(0)}(\mathbf{r}) + \sum_{i > 0} \alpha_i \Delta f_i(\mathbf{r}) \quad (4)$$

where  $\Delta f_i(\mathbf{r})$  is defined as the state dual descriptor for excited state  $i$  (or state-specific dual descriptor)

$$\Delta f_i(\mathbf{r}) \equiv \rho_R^{(i)}(\mathbf{r}) - \rho_R^{(0)}(\mathbf{r}) \quad (5)$$

As can be seen,  $\Delta f_i(\mathbf{r})$  is defined as the difference between the various excited state electron densities of this complex and the ground state electron density of the reactant complex. These state-specific dual descriptors, already in use to study electron transfer<sup>33,37,38</sup>, are generalization of the usual or “traditional” dual descriptor, introduced as the derivative of the Fukui function<sup>39</sup> with respect to the number of electrons at constant external potential.

$$f^{(2)}(\mathbf{r}) = \left(\frac{\partial f(\mathbf{r})}{\partial N}\right)_v \approx f^+(\mathbf{r}) - f^-(\mathbf{r}) \quad (6)$$

The Fukui function was introduced as the derivative of the electronic chemical potential  $\mu$  with respect to the external potential and is connected through a Maxwell relation with the change of the electron density with respect to the number of electrons

$$f(\mathbf{r}) = \left[ \frac{\delta\mu}{\delta v(\mathbf{r})} \right]_N = \left( \frac{\partial \rho(\mathbf{r})}{\partial N} \right)_v \quad (7)$$

The electronic chemical potential is the derivative of the energy with respect to the number of electrons and has been identified as the negative of the electronegativity  $\chi$ .

$$\mu = \left( \frac{\partial E}{\partial N} \right)_v = -\chi \quad (8)$$

Due to the discontinuity of  $\rho(\mathbf{r})$  with respect to the number of electrons, the left and right side derivative of Eq. (7) will be different and will be associated with the Fukui function, for an  $N$ -electron system, for an electrophilic ( $f^-(\mathbf{r})$ ) and a nucleophilic ( $f^+(\mathbf{r})$ ) attack respectively

$$f^-(\mathbf{r}) = \left( \frac{\partial \rho(\mathbf{r})}{\partial N} \right)_v^- = \rho_N(\mathbf{r}) - \rho_{N-1}(\mathbf{r}) \quad (9)$$

$$f^+(\mathbf{r}) = \left( \frac{\partial \rho(\mathbf{r})}{\partial N} \right)_v^+ = \rho_{N+1}(\mathbf{r}) - \rho_N(\mathbf{r}) \quad (10)$$

In these equations,  $\rho_N(\mathbf{r})$ ,  $\rho_{N+1}(\mathbf{r})$  and  $\rho_{N-1}(\mathbf{r})$  correspond to the electron densities of the  $N$ ,  $N+1$  and  $N-1$  electron system respectively.

Returning to Eq. (4), it can easily be seen that the change in the electron density  $\Delta\rho(\mathbf{r})$  when going from the reactant complex to the transition state of the reaction can be written as

$$\Delta\rho(\mathbf{r}) \equiv \rho_{TS}^{(0),ext}(\mathbf{r}) - \rho_R^{(0)}(\mathbf{r}) = \sum_{i>0} \alpha_i \Delta f_i(\mathbf{r}) \quad (11)$$

which, in principle, is an exact expression. This expression decomposes the density variation from the initial state of the reaction to the transition state in a series of contributions from the different state-specific dual descriptors of the reactant complex. It should indeed be stressed that the state-specific dual descriptors involved should necessarily be evaluated for the reactant complex in the initial stages of the reaction.

This expression also allows a nice physical interpretation of the density deformation upon a chemical reaction. Eq. (11) decomposes the total deformation density in a series of density changes corresponding to excitations in the reactant complex, which, in view of the earliness of this complex, will largely correspond to either intra-fragment excitations and/or excitations between the two interacting fragments. It is tempting to associate the former to the polarization contribution of the two charge clouds when they are perturbed by the approaching reagents, whereas the latter should be associated to charge transfer between the fragments. This is depicted in Figure 1.

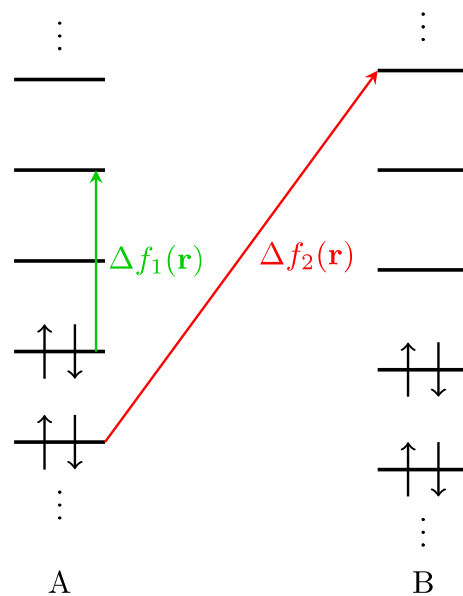


**Figure 1.** Intra-fragment (green) and inter-fragment (red) state specific dual descriptors for the interaction between two fragments A and B.

The conceptual DFT framework also allows the derivation of an expression for the density change for the isolated reactants, say A and B, to the transition state of the reaction which can be derived as follows. The density change of both A and B can be expressed to first order as

$$\rho_A(\mathbf{r}) = \rho_A^0(\mathbf{r}) + \left( \frac{\partial \rho_A(\mathbf{r})}{\partial N_A} \right)_{v_A} \Delta N_A + \int \left[ \frac{\delta \rho_A(\mathbf{r})}{\delta v_A(\mathbf{r}')} \right]_{N_A} \Delta v_A(\mathbf{r}') d\mathbf{r}' \quad (12)$$

and

$$\rho_B(\mathbf{r}) = \rho_B^0(\mathbf{r}) + \left( \frac{\partial \rho_B(\mathbf{r})}{\partial N_B} \right)_{v_B} \Delta N_B + \int \left[ \frac{\delta \rho_B(\mathbf{r})}{\delta v_B(\mathbf{r}')} \right]_{N_B} \Delta v_B(\mathbf{r}') d\mathbf{r}' \quad (13)$$

These equations, in addition to the Fukui function, now also contain the linear response function  $\chi(\mathbf{r}, \mathbf{r}')$ . This latter descriptor has been proven quite helpful to characterize electronic effects such as inductive and mesomeric effects<sup>40-42</sup>.

$$\chi(\mathbf{r}, \mathbf{r}') \equiv \left[ \frac{\delta \rho(\mathbf{r})}{\delta v(\mathbf{r}')} \right]_N \quad (13)$$

As can be seen, the first term describes the charge transfer to/from the fragments upon their evolution to the transition state, whereas the second term describes the polarization of their electron densities due to the perturbation in the external potential.

The total density of the transition state can thus be written as

$$\begin{aligned} \rho_{TS}(\mathbf{r}) = \rho_A(\mathbf{r}) + \rho_B(\mathbf{r}) = \rho_A^0(\mathbf{r}) + \rho_B^0(\mathbf{r}) \\ + f_A(\mathbf{r})\Delta N_A + f_B(\mathbf{r})\Delta N_B + \int \chi_A(\mathbf{r}, \mathbf{r}')\Delta v_A(\mathbf{r}')d\mathbf{r}' + \int \chi_B(\mathbf{r}, \mathbf{r}')\Delta v_B(\mathbf{r}')d\mathbf{r}' \end{aligned} \quad (14)$$

or

$$\Delta \rho(\mathbf{r}) = f_A(\mathbf{r})\Delta N_A + f_B(\mathbf{r})\Delta N_B + \int \chi_A(\mathbf{r}, \mathbf{r}')\Delta v_A(\mathbf{r}')d\mathbf{r}' + \int \chi_B(\mathbf{r}, \mathbf{r}')\Delta v_B(\mathbf{r}')d\mathbf{r}' \quad (15)$$

Now writing

$$\Delta N = \Delta N_A = -\Delta N_B \quad (16)$$

yields

$$\Delta \rho(\mathbf{r}) = f_A(\mathbf{r})\Delta N - f_B(\mathbf{r})\Delta N + \int \chi_A(\mathbf{r}, \mathbf{r}')\Delta v_A(\mathbf{r}')d\mathbf{r}' + \int \chi_B(\mathbf{r}, \mathbf{r}')\Delta v_B(\mathbf{r}')d\mathbf{r}' \quad (17)$$

If it is considered in the course of the reaction that electrons are transferred from B to A, the density response towards charge transfer of A will be governed by  $f_A^+(\mathbf{r})$  and the density response for B by  $f_B^-$

$$\Delta\rho(\mathbf{r}) = (f_A^+(\mathbf{r}) - f_B^-(\mathbf{r}))\Delta N + \int \chi_A(\mathbf{r}, \mathbf{r}')\Delta v_A(\mathbf{r}')d\mathbf{r}' + \int \chi_B(\mathbf{r}, \mathbf{r}')\Delta v_B(\mathbf{r}')d\mathbf{r}' \quad (18)$$

The quantity  $f_A^+(\mathbf{r}) - f_B^-(\mathbf{r})$  can now be considered as an approximation for the dual descriptor at the initial stages of the reaction, so that, finally,

$$\Delta\rho(\mathbf{r}) \approx f^{(2)}(\mathbf{r})\Delta N + \int \chi_A(\mathbf{r}, \mathbf{r}')\Delta v_A(\mathbf{r}')d\mathbf{r}' + \int \chi_B(\mathbf{r}, \mathbf{r}')\Delta v_B(\mathbf{r}')d\mathbf{r}' \quad (19)$$

showing that, when  $\Delta\rho(\mathbf{r})$  is considered between the TS and the isolated reactants, the charge transfer between the two fragments is modulated by the dual descriptor. This again points to the role of this quantity in determining the density deformation upon the evolution towards the transition state.

The decomposition described above bears resemblance with the Natural Orbitals for Chemical Valence (NOCV) introduced by Mittoraj, Michalak and Ziegler<sup>43,44</sup>. These NOCVs,  $\psi_i$ , are defined as the eigenvectors that diagonalize the deformation density  $\Delta\rho(\mathbf{r})$

$$\Delta\rho(\mathbf{r}) = \sum_{i=1}^M v_i \psi_i^2(\mathbf{r}) \quad (20)$$

In this case,  $\Delta\rho(\mathbf{r})$  is defined as the density change between two interacting fragments and these two isolated fragments in the geometry they adopt in the complex. This deformation density can then be expressed as a sum of pairs of complementary eigenfunctions ( $\psi_k, -\psi_k$ ) corresponding to the eigenvalues  $v_k$  and  $-v_k$ .

$$\Delta\rho(\mathbf{r}) = \sum_{k=1}^{M/2} v_k [\psi_k^2(\mathbf{r}) - \psi_{-k}^2(\mathbf{r})] \quad (21)$$

As such, the eigenvalue  $v_k$  is the number of electrons that is transferred from orbital  $\psi_k$  to  $-\psi_k$  upon bond formation. The density deformation,  $\Delta\rho_k(\mathbf{r})$ , represented by a complementary NOCV pair, can thus be expressed as

$$\Delta\rho_k(\mathbf{r}) = v_k [\psi_k^2(\mathbf{r}) - \psi_{-k}^2(\mathbf{r})] \quad (21)$$

In addition, a method to obtain interaction energies associated to each of these density deformations has been put forward.

The aim of the present paper is to show how much similar the information provided by the NOCVs and the state specific dual descriptors (SSDDs) are. In this context, a NOCV stabilization energy counterpart is also required. It is obvious that the electron density distortion energy needed to change the density, on each physical point, by  $\Delta\rho(\mathbf{r})$  at constant external potential, is somehow comparable to the NOCVs stabilizing energy. A DFT based derivation for calculating such an energy is given in annex, the actual computation of such quantity would be quite difficult to perform though.

So for the time being, we propose a different and more suitable, even though more approximate, way to evaluate the electron density distortion energy. The density deformation energy reads:

$$\Delta E_{\text{distortion}} = E_v[\rho_f] - E_v[\rho_i] \quad (22)$$

Starting from Eq. (22) and assuming the electron density deformation can be approximately computed through a particular state specific dual descriptor, then the electron distortion energy can be calculated using

$$\Delta E_{\text{distortion}} = E_v[\rho_i^{\text{exc}}] - E_v[\rho_0] \approx \Delta E_i^{\text{exc}} \quad (23)$$

in which  $\rho_i^{\text{exc}}$  stands for the density of the specific excited state  $i$ , while  $\rho_0$  is the ground state density. This energy can therefore be roughly approximated by the excitation energy  $\Delta E_i^{\text{exc}}$ . Indeed, the excitation energy only differs from Eq. (23) by the way the exchange correlation functional is computed for the first term of the right hand side. As a consequence, the excitation energy corresponding to each state specific dual descriptor can be expected to yield a fair measure of the energy needed to distort the electron density by  $\Delta f_i(\mathbf{r})$ . In this framework, the first state specific dual descriptor would be the easiest way to modify the electron density and the first excitation energy a fair approximation of the energy needed to make this modification happen. However, distortion energy is not the only interesting parameter for that purpose. The oscillator strength is another quantity that might also be relevant<sup>45</sup>. The oscillator strength ( $f_{mn}$ ) for a transition between two states  $m$  and  $n$  is computed through the following equation:

$$f_{mn} = \frac{2m_e}{3q\hbar^2} (E_n - E_m) \mu_{mn}^2 \quad (24)$$

in which  $m_e$  stands for the electron mass,  $q$  the electron charge.  $E_n$  and  $E_m$  are the energies of states  $m$  and  $n$  respectively while  $\mu_{mn}$  is the associated optical transition dipole moment. The oscillator strength characterizes the intensity of a transition between two states, which is related to the transition rate. The next step is to assume that it also carries information about the likelihood to distort the electron density from state  $m$  to state  $n$ . Thus, a SSDD associated to an excitation with an oscillator strength of zero could suggest that this way to distort the density is quite unlikely, while one might be confident in an electron density evolution associated with a big oscillator strength. Another interesting point is the relation between the transition dipole moment between two quantum states and the overlap integral between these two states. The molecular dipole moment is actually the sum of the electron moment ( $\mu_e$ ) and the nuclei moment ( $\mu_N$ ). The nuclei moment does not depend on electron coordinates. Assuming the nuclei conformation is barely changed so that the electron wave-functions remains almost the same during the excitation process :

$$\mu_{mn} = \langle \Psi_m | \mu_N + \mu_e | \Psi_n \rangle = \mu_N \mathbf{S}_{mn} + \langle \Psi_m | \mu_e | \Psi_n \rangle \quad (25)$$

Thus the transition dipole moment is related to the integral overlap. As a consequence, the higher the dipole moment, the better the spatial overlap between the two quantum states, therefore the easier the charge transfer will be. A weak transition dipole moment does not necessarily indicate a nil charge transfer.

All these assumptions are tested from several chemical relevant situations in the next part.

### Computational Details

All the molecules have been fully optimized at B3LYP/6-31+G(d) level of theory with Gaussian 09 Rev B.02<sup>46</sup>. Vibrational frequencies have been computed to characterize transition states and stationary points. IRC calculations have also been performed to obtain chemical pathways. The State Specific Dual Descriptors (SSDD) of  $i^{\text{th}}$  order have been calculated as the difference between the density of the  $i^{\text{th}}$  excited state and the density of the ground state. The excited state densities have been obtained through TDDFT calculations limited to the first 10 excitations. The cube file associated to each density has been computed using the “medium” grid which gives a fair balance between accuracy and computational time. The NOCVs have been calculated at the transition state of each chemical reactions, except for the formation of the  $\text{NH}_3\text{-BH}_3$  complex (details given in the text), using ADF 2013.01<sup>47</sup> on Gaussian geometries. The same grid quality as for the dual descriptor has been applied for NOCVs. To facilitate the comparison between the NOCVs and the State Specific Dual Descriptors, positive basins are colored in cyan while negative basins are colored in orange. All the energies are given in kcal/mol. In all pictures, the acronym IDT stands for Isosurface Density Threshold. This acronym is recalled in the caption of the first picture.

## Results and Discussion

The theoretical development makes a formal relation between the dual descriptor, either usual or state specific, and the NOCVs. In this part, some computational evidences are provided to support this assumption. The investigated chemical reactions are the formation of the  $\text{NH}_3\text{-BH}_3$  Lewis acid-Lewis base complex from borane and ammonia, the nucleophilic substitution of chloromethane by chloride, and two [4+2] cycloadditions. In each example, the dual descriptor computed for the pre-reactive complexes of these reactions is compared to the results of a NOCV analysis performed on the transition state. It will be seen that, in general, both concept match surprisingly well.

### 1. $\text{NH}_3\text{-BH}_3$

The first reaction investigated is the formation of the  $\text{NH}_3\text{-BH}_3$  complex from borane and ammonia. As this chemical phenomenon occurs without transition state, the NOCV analysis has been performed on the product. The State Specific Dual Descriptors (SSDDs) have been computed on a constrained geometry in which the boron and the nitrogen atom are kept at 4 Å distance and both fragments are oriented in the reactive conformation. Both SSDD and NOCVs maps are represented in Figure 2a and Figure 2b respectively. As can be expected, only one NOCV pair is prevalent. The associated stabilizing orbital energy is 65.3 kcal/mol. As expected, this NOCV pair indicates that the electron density flows from the nitrogen atom of ammonia (orange basin) towards the boron atom (blue basin) of borane. This is in perfect line with the classical rationale of the reaction as the formation of a dative bond between the lone pair of nitrogen and the empty  $2p_z$  orbital of boron. The former

is the HOMO of the system while the latter is its LUMO. The first SSDD has also been computed and is displayed in Figure 2a. As expected, the SSDD predicts that nitrogen is nucleophilic and therefore loses electron density during the process, while the boron is electrophilic, and hence acquires density during the reaction. Interestingly the usual dual descriptor (not represented here), computed as the difference in densities between the LUMO and the HOMO, is identical to the first SSDD. The only notable difference is an orbital relaxation torus located around the boron atom. Pictures of the abovementioned NOCV pair and SSDD are also quite similar and overall provide the same chemical information. It is worth noticing that the oscillator strength associated with the first excitation (involved in the calculation of the 1<sup>st</sup> SSDD) is 0.0682 while the oscillator strengths of 2<sup>nd</sup> and 3<sup>rd</sup> excitations vanish. The 1<sup>st</sup> SSDD seems the only relevant dual descriptor needed to characterize the evolution of the electron density. Thus, for the formation of  $\text{NH}_3\text{-BH}_3$ , both the first NOCV pair and the SSDD are able to characterize the evolution of the electron density and provide quite similar chemical information. Besides the NOCV and SSDD maps are very similar.

## 2. $\text{S}_{\text{N}}2$ reactions

Two prototypical bimolecular nucleophilic substitution reactions<sup>48</sup> ( $\text{S}_{\text{N}}2$ ) have been investigated. The reactions involve chloromethane (resp. bromomethane) as the substrate in which the halogen atom is substituted by a chlorine ion. NOCV pairs have been calculated for the transition state. The same methodology has been applied for this system as for the previous one. In addition, the reactants have been fully optimized with the distance between the attacking chloride and the carbon frozen at

4 Å. The results are displayed in Figure 3 and in Figure 4. Again, only one NOCV pair is dominant with an energy of 39.5 kcal/mol. (respectively 40.7 kcal/mol for bromomethane reacting with chloride). In both cases, the NOCV pair (Figure 3d and Figure 4d) corresponds to a charge transfer from one of the four lone pairs of the chloride nucleophile (orange basin) towards the carbon atom of the substrate (blue basin). It is interesting to note that the leaving chlorine gets extra density during the course of the reaction.

Three State Specific Dual Descriptors have been calculated. They are all displayed in Figures 3a, 3b, 3c and 4a, 4b, 4c. The first two SSDDs (Figure 3a, 3b and 4a, 4b) originate from degenerated excitations, both at 3.41 eV (respectively 2.84 eV for bromomethane) and exhibit almost nil oscillator strengths with a value around  $3 \cdot 10^{-4}$  (respectively  $2 \cdot 10^{-3}$  for bromomethane system). It is very unlikely that these SSDDs correspond to important electron density distortion reactive modes. The usual dual descriptor computed from frontier densities is very similar to these first two SSDDs. In this particular case, the usual dual descriptor fails to characterize the chemical reactivity. On the other hand, the third SSDD has a much bigger oscillator strength of  $4 \cdot 10^{-2}$  (respectively  $8 \cdot 10^{-2}$  for bromomethane system) and originates from an excitation of 3.48 eV which is quite close to the first two excitations. This SSDD corresponds to an inter-fragment electron excitation from one chloride lone pair toward the  $\sigma^*_{\text{C-Cl}}$  anti-bonding orbital (resp.  $\sigma^*_{\text{C-Br}}$ ). This SSDD provides the same information as the NOCV pair. Indeed, the orange basin located on the attacking chloride represents the loss of density this atom undergoes during the chemical event, while the blue basin on the carbon of the substrate, either chloromethane or bromomethane, describes the gain of density resulting in the formation of the

chemical bond. The SSDD is also able to predict the gain of density the leaving group gets during the course of the process, though the chosen IDT on Figures 3 and 4 does not reveal the corresponding blue basin (lowering the IDT to 0.006 a.u. would make it visible). One can argue that, at infinite distances (much more than 4Å), the difference in energy between the three first SSDD (3.48 vs 3.41) should vanish, this difference being reasonably attributed to a weak interaction between Cl and CH<sub>3</sub>Cl. However, at distances greater than 4 Å, convergence troubles appear, typically do to self-interaction errors<sup>49</sup>.

It is also worth noticing that by comparison with the usual dual descriptor, the SSDDs are more robust. Indeed, the oscillator strengths are good indicators of the likelihood of the corresponding electron distortion mode. Thus, it is quite easy to determine which SSDD is more likely to represent the electron density evolution.

### 3. Diels-Alder Cycloadditions

In this section, two kinds of Diels-Alder cycloadditions have been investigated<sup>50</sup>. Firstly, the formation of cyclohexene has been studied. Next, to probe the effect of substitution, the cycloaddition between butadiene and dicyanoethane has been studied.

#### *a. Butadiene-ethene cycloaddition.*

For the butadiene-ethylene system, two main NOCV pairs, depicted in Figure 5a and 5b, are observed. The stabilization energies associated with the two NOCV pairs are 23.7 and 23.0 kcal/mol respectively. They are interestingly lying quite close to each other. As can be seen from Figure 5a, the first NOCV pair characterizes the charge transfer from the dienophile, in this case the ethylene, acting as nucleophile to the

diene, acting as the electrophile. It can be seen that the orbitals associated with this NOCV pair roughly correspond to the HOMO of ethylene and the LUMO of butadiene. The second NOCV pair, with almost the same energy as the first pair, describes the reverse process, a donation from the diene toward the dienophile. In this case, the corresponding orbitals are the other pair of frontier orbitals, namely the HOMO of butadiene and the LUMO of ethylene. The fact that the two main NOCVs pairs exhibit the same energy can be expected since the two pairs of frontier orbitals have roughly the same energy gap.

Three State Specific Dual Descriptors have been calculated and are displayed in Figure 6. As for the previous system, the SSDDs have been computed for a pre-reactive complex in which the distances between reacting atoms are set at 4 Å. The usual Dual Descriptor (not shown) highly resembles the first SSDD. As can be seen in Figure 6, this very first SSDD does not characterize charge transfer between the fragments. It indeed describes an intra-fragment excitation and can thus be assumed that it constitutes the easiest way to polarize the electron density in the pre-reactive complex. The fact that the first SSDD and the dual descriptor densities are mainly located on the butadiene fragment is due to the fact that the frontier orbital energies of butadiene lie within the energy gap of the frontier orbitals of ethylene. Contrarily to the previous examples, the very first SSDD properly describe the main reactive mode for this reaction. The main product isolated after a tentative reaction between butadiene and ethylene is not cyclohexene but 4-vinyl-cyclohexene. The latter product is formed by the cycloaddition between two butadiene molecules. The first SSDD just shows that butadiene is more reactive than ethylene and tends to react with another butadiene molecule. The rationalization of this chemical behavior through the use of the dual descriptor has already been described in several papers<sup>14,51,52</sup>.

The second and third SSDDs correspond to excitation energies of 5.41 and 5.56 eV respectively. Those energies are quite close to each other and somehow reflect the quasi degeneracy of the NOCVs pair energies. Their oscillator strengths are  $1.10^{-2}$  and  $5.10^{-2}$  respectively. It appears quite clearly that those two SSDDs provide the same kind of information as the NOCV pairs. Both SSDDs arise from inter-fragment excitations. The second SSDD looks like the first NOCV pair and predicts the charge transfer from ethene toward butadiene. On the contrary, the third SSDD describes a back-donation from the butadiene to ethene. The energy order is the same as for the NOCV pairs. The donation from ethene toward butadiene corresponds to a lower excitation energy than the back-donation.

To investigate the effects of the distance variation between the reacting atoms, the SSDDs have also been computed for a distance of 2.8 Å between the reacting molecules, which however can still be considered to belong to the reactant region<sup>53</sup>. The first three SSDDs are displayed in Figure 7. Three main differences occur when one compares the results at 2.8 Å with the results at 4 Å. First, the SSDDs order differs. Indeed, the first two SSDDs swap. The one looking like the first NOCV pair, namely the second SSDD at 4 Å, now turns out to be the first SSDD at 2.8 Å. Finally, one observes an increase in the oscillator strength. Indeed, for the 2.8 Å system, they are from 3 to 10 times higher than for the 4 Å system. This can be explained by the better overlap between the two quantum states involved in the electronic transition. The excitation energies and the oscillator strength for both systems are gathered in Table 1.

*b. Butadiene-1,1-dicyanoethene cycloaddition*

The same methodology has been applied to the cycloaddition of butadiene with 1,1-dicyanoethene. Introducing substitution on the dienophile results in the loss of synchronicity of the reaction. Indeed, the bond between a butadiene carbon and the unsubstituted carbon of dicyanoethene is created first. Then the reaction continues by forming the bond between the other terminal carbon of butadiene with the substituted carbon of dicyanoethane. The chemical process remains concerted though. Again, one observes two main NOCV pairs, displayed in Figure 8. The first NOCV pair has a stabilization energy of 44.5 kcal/mol and constitutes the predominant one. The second NOCV pair exhibits a lower stabilizing energy of 18.3 kcal/mol. The information provided by these two NOCV pairs is very similar to that of butadiene-ethene system. Since cyano groups are electron withdrawing, they stabilize the whole set of orbitals. As a consequence, the energy gap between the HOMO of butadiene and the LUMO of ethylene decreases, thus generating a higher stabilization energy. Another quite important difference is the asymmetry. Indeed, in both NOCV pairs, the electron density transfer between the unsubstituted carbon of 1,1-dicyanoethene and one carbon of butadiene is clearly observed. Unexpectedly, the charge transfer leading to the formation of the other bond, namely the one between the substituted carbon of 1,1-dicyanoethene and the other terminal carbon of butadiene, is not observed on the two main NOCVs. As the NOCVs have been computed at the Transition State (TS), one can conclude that this bond formation happens after the TS.

Again, the three first SSDDs have been computed and are represented in Figure 9. The usual dual descriptor, not shown, is very similar to the first SSDD. It is easy to see that the first SSDD resembles the main NOCV. The prediction of the reacting site is easy, since the SSDD condensed value on the electrophilic basin located below and

above the unsubstituted carbon of 1,1-dicyanoethene (0.21 a.u) is higher than that of the substituted carbon (0.13 a.u). The future asymmetry of the TS is well predicted by the first SSDD. However, it appears clearly that none of the SSDD is able to provide the same information as the second NOCV. To tackle this problem, it has been supposed that the second NOCV reflects a late phenomenon that cannot be predicted from the reactant complex. So the SSDDs have been again computed for the geometry of the maximum reaction force<sup>54,55,56</sup>, almost at the inflexion point on the Potential Energy Surface (PES). It is supposed that being closer to the TS, the SSDD corresponding to the second NOCV would eventually show. The SSDDs calculated for this geometry are displayed in Figure 10. As can be seen, the first SSDD remains unchanged. On the contrary the second SSDD appears very different. As can be seen for the second SSDD, although not completely identical to the second NOCV, the chemical information on the reacting carbon, namely the unsubstituted carbon of 1,1-dicyanoethene and one terminal carbon of butadiene, is identical. Indeed, the terminal carbon of butadiene exhibits an electrophilic behavior, while the unsubstituted carbon of 1,1-dicyanoethene acts as nucleophile. This behavior totally matches the analysis for the second NOCV that indicates a loss of density of the latter and the gain of density of the former. So, even though the two maps are not totally identical, the chemical information provided by both is equivalent.

### Conclusions

In this paper, a formal link between the Natural Orbitals for Chemical Valence (NOCV) and both the “usual” dual descriptor and the state specific dual descriptors (SSDD) is made. This physical development is based upon a Taylor series expansion of the electron density variation at the onset of a chemical reaction. The relation

between the NOCV stabilization energies and the excitation energies attached to each state specific dual descriptor is also discussed. In addition, the role of the oscillator strengths for rationalizing the likelihood of the electron density evolution is analyzed. These theoretical considerations have been tested for different chemical reactions like the bimolecular nucleophilic substitution or Diels Alder cycloaddition. It appears that in all cases, the main NOCV matches one of the first three State Specific Dual Descriptor. It appears that from a basic analysis of the excitation type and the oscillator strength, the SSDD matching the NOCV can be predicted *a priori*. In addition, some examples show that the usual dual descriptor is not always up to a proper description of the chemical reactivity. On the other hand, the state specific dual descriptor proves its flexibility.

### **Acknowledgements**

The research benefited from the support of Aviesan ITMO Cancer within the “Cancer Plan 2009–2013” and the application of Action 3.3. A. F.D.P. wishes to acknowledge the University Claude Bernard Lyon 1 for an invited professorship during the month of May of 2014. P.G. and F.D.P wish to thank the Research Foundation-Flanders (FWO) and the Free University of Brussels (VUB) for continuous support of their research group, specially mentioning the Strategic Research Program awarded to the ALGC group by the VUB which started on January 1, 2013. C.M thanks the University of Lyon 1 for the BQR grant 2013.

### **Appendix**

The annex is dedicated to the derivation of a DFT expression of the electron density distortion energy. Its relation with excitation energies is discussed.

The energy needed to distort the electron density at constant external potential is given by:

$$\Delta E_{\text{distortion}} = E_{\nu}[\rho_f] - E_{\nu}[\rho_i] \quad (26)$$

In Eq. (26),  $\nu$  represents the common external potential to both states.  $\rho_i$  and  $\rho_f$  are respectively the electron densities of initial and final states. Using the regular electron density functional energy, Eq. (26) becomes:

$$\Delta E_{\text{distortion}} = \int [\rho_f(\mathbf{r}) - \rho_i(\mathbf{r})] \nu(\mathbf{r}) d\mathbf{r} + F_{\text{HK}}[\rho_f] - F_{\text{HK}}[\rho_i] \quad (27)$$

in which  $F_{\text{HK}}[\rho_f]$  is the universal Hohenberg-Kohn functional. If one assumes that the final electron density is not that different from the initial electron density, then using a second order Taylor's development, one gets:

$$\Delta E_{\text{distortion}} = \int \Delta\rho(\mathbf{r}) \nu(\mathbf{r}) d\mathbf{r} + \int \left( \frac{\delta F}{\delta\rho(\mathbf{r})} \right)_{\rho_i} \Delta\rho(\mathbf{r}) d\mathbf{r} + \frac{1}{2} \iint \left( \frac{\delta^2 F}{\delta\rho(\mathbf{r})\delta\rho(\mathbf{r}')} \right)_{\rho_i} \Delta\rho(\mathbf{r}) \Delta\rho(\mathbf{r}') d\mathbf{r} d\mathbf{r}' \quad (28)$$

In Eq. (28),  $\Delta\rho(\mathbf{r})$  denotes the difference between final and initial densities  $\Delta\rho(\mathbf{r}) = \rho_f(\mathbf{r}) - \rho_i(\mathbf{r})$ . Still in Eq. (24), the subscript  $\rho_i$  indicates that the derivative of the Hohenberg-Kohn functional with respect to the electron density is evaluated for

the initial density. Then, by combining the two first terms of the right hand side of Eq. (24), one obtains:

$$\Delta E_{\text{distortion}} = \int \Delta\rho(\mathbf{r}) \left[ v(\mathbf{r}) + \left( \frac{\delta F}{\delta\rho(\mathbf{r})} \right)_{\rho_i} \right] d\mathbf{r} + \frac{1}{2} \iint \left( \frac{\delta^2 F}{\delta\rho(\mathbf{r})\delta\rho(\mathbf{r}')} \right)_{\rho_i} \Delta\rho(\mathbf{r})\Delta\rho(\mathbf{r}') d\mathbf{r}d\mathbf{r}' \quad (29)$$

In this equation, the expression between brackets in the first hand side term is easily identified as the chemical potential of the initial state and therefore Eq. (29) becomes:

$$\Delta E_{\text{distortion}} = \mu_i \int \Delta\rho(\mathbf{r}) d\mathbf{r} + \frac{1}{2} \iint \left( \frac{\delta^2 F}{\delta\rho(\mathbf{r})\delta\rho(\mathbf{r}')} \right)_{\rho_i} \Delta\rho(\mathbf{r})\Delta\rho(\mathbf{r}') d\mathbf{r}d\mathbf{r}' \quad (30)$$

Since the number of electrons remains the same in the initial and final state, the first hand side term of Eq. (30) vanishes and one eventually gets:

$$\Delta E_{\text{distortion}} = \frac{1}{2} \iint \left( \frac{\delta^2 F}{\delta\rho(\mathbf{r})\delta\rho(\mathbf{r}')} \right)_{\rho_i} \Delta\rho(\mathbf{r})\Delta\rho(\mathbf{r}') d\mathbf{r}d\mathbf{r}' \quad (31)$$

Assuming  $\Delta\rho(\mathbf{r})$  is well represented by a weighted combination of state specific excited states ( $\Delta\rho(\mathbf{r}) = \sum_i \alpha_i \Delta f_i(\mathbf{r})$ , see Eq. 11). In this case, Eq. (31) reads:

$$\Delta E_{\text{distortion}} = \frac{1}{2} \iint \left( \frac{\delta^2 F}{\delta\rho(\mathbf{r})\delta\rho(\mathbf{r}')} \right)_{\rho_i} \sum_i \alpha_i \Delta f_i(\mathbf{r}) \sum_j \alpha_j \Delta f_j(\mathbf{r}') d\mathbf{r}d\mathbf{r}' \quad (32)$$

Eq. (32) can be rearranged as:

$$\begin{aligned} \Delta E_{\text{distortion}} = & \frac{1}{2} \iint \left( \frac{\delta^2 F}{\delta \rho(\mathbf{r}) \delta \rho(\mathbf{r}')} \right)_{\rho_i} \sum_i \alpha_i^2 \Delta f_i(\mathbf{r}) \Delta f_i(\mathbf{r}') d\mathbf{r} d\mathbf{r}' \\ & + \iint \left( \frac{\delta^2 F}{\delta \rho(\mathbf{r}) \delta \rho(\mathbf{r}')} \right)_{\rho_i} \sum_i \sum_{j>i} \alpha_i \alpha_j \Delta f_i(\mathbf{r}) \Delta f_j(\mathbf{r}') d\mathbf{r} d\mathbf{r}' \end{aligned} \quad (33)$$

In cases where the electron density variation is well represented by a single state specific dual descriptor ( $\alpha_i = 1; \forall j \neq i \alpha_j = 0$ ), Eq. (33) becomes:

$$\Delta E_{\text{distortion}} = \frac{1}{2} \iint \left( \frac{\delta^2 F}{\delta \rho(\mathbf{r}) \delta \rho(\mathbf{r}')} \right)_{\rho_i} \Delta f_i(\mathbf{r}) \Delta f_i(\mathbf{r}') d\mathbf{r} d\mathbf{r}' \quad (34)$$

In the few studied examples, it will be seen that one generally needs at best only one state specific dual descriptor and in the worse cases two state specific dual descriptors. Therefore, Eq. (34) is a fair measure of the energy needed to distort the electron density at each point by  $\Delta f_i(\mathbf{r})$ . Identifying the hardness kernel, Eq. (34) now reads:

$$\Delta E_{\text{distortion}} = \frac{1}{2} \iint \eta(\mathbf{r}, \mathbf{r}') \Delta f_i(\mathbf{r}) \Delta f_i(\mathbf{r}') d\mathbf{r} d\mathbf{r}' \quad (35)$$

The hardness kernel is traditionally decomposed into two terms: a Hartree term translating the electrostatic repulsion between electron and another term gathering the kinetic and the exchange-correlation energy:

$$\Delta E_{\text{distortion}} = \frac{1}{2} \left[ \iint \frac{\Delta f_i(\mathbf{r}) \Delta f_i(\mathbf{r}')}{|\mathbf{r} - \mathbf{r}'|} d\mathbf{r} d\mathbf{r}' + \iint R(\mathbf{r}, \mathbf{r}') \Delta f_i(\mathbf{r}) \Delta f_i(\mathbf{r}') d\mathbf{r} d\mathbf{r}' \right] \quad (36)$$

It is generally assumed that the Hartree term is predominant<sup>57,58</sup> and hence that Eq. (36) can be reduced to:

$$\Delta E_{\text{distortion}} \approx \frac{1}{2} \iint \frac{\Delta f_i(\mathbf{r}) \Delta f_i(\mathbf{r}')}{|\mathbf{r} - \mathbf{r}'|} d\mathbf{r} d\mathbf{r}' \quad (37)$$

Eq. (37) is therefore only a rough evaluation of the energy needed to change the electron density by  $\Delta f_i(\mathbf{r})$ , supposedly when the kinetic, exchange and correlation can be overlooked with respect to the electrostatic energy. But it would be very difficult to assess when this approximation is justified. Besides, the use of Eq. (36) to express the distortion energy supposes the knowledge of a good approximation for the kinetic and exchange correlation term, which is not the case so far.

## References

1. P. Geerlings, F. De Proft, and W. Langenaeker, *Chem. Rev.*, 2003, **103**, 1793–873.
2. H. Chermette, *J. Comput. Chem.*, 1998, **20**, 129–154.
3. J. L. Gázquez, *J. Mex. Chem. Soc.*, 2008, **52**, 3–10.
4. P. W. Ayers and R. G. Parr, *J. Am. Chem. Soc.*, 2001, **123**, 2007–17.
5. R. P. Iczkowski and J. L. Margrave, *J. Am. Chem. Soc.*, 1961, **83**, 3547–3551.
6. R. G. Parr, R. A. Donnelly, M. Levy, and W. E. Palke, *J. Chem. Phys.*, 1978, **68**, 3801–3807.
7. L. Tarko and M. V Putz, 2010, 487–495.
8. R. G. Parr and R. G. Pearson, *J. Am. Chem. Soc.*, 1983, **105**, 7512–7516.
9. R. G. Pearson, *J. Chem. Sci.*, 2005, **117**, 369–377.
10. R. G. Pearson, *J. Am. Chem. Soc.*, 1988, **110**, 7684–7690.
11. W. Yang and R. G. Parr, *Proc. Natl. Acad. Sci. U. S. A.*, 1985, **82**, 6723–6726.
12. C. Morell, A. Grand, and A. Toro-Labbé, *J. Phys. Chem. A*, 2005, **109**, 205–212.
13. C. Morell, A. Grand, and A. Toro-Labbé, *Chem. Phys. Lett.*, 2006, **425**, 342–346.
14. C. Morell, P. W. Ayers, A. Grand, S. Gutiérrez-Oliva, and A. Toro-Labbé, *Phys. Chem. Chem. Phys.*, 2008, **10**, 7239–7246.
15. C. Cárdenas, N. Rabi, P. W. Ayers, C. Morell, P. Jaramillo, and P. Fuentealba, *J. Phys. Chem. A*, 2009, **113**, 8660–8667.
16. J. I. Martínez, J. L. Moncada, and J. M. Larenas, *J. Mol. Model.*, 2010, **16**, 1825–32.
17. R. G. Parr, L. von Szentpaly, and S. Liu, *J. Am. Chem. Soc.*, 1999, **121**, 1922–1924.
18. P. K. Chattaraj, U. Sarkar, and D. R. Roy, *Chem. Rev.*, 2006, **106**, 2065–91.

19. C. Morell, V. Labet, A. Grand, and H. Chermette, *Phys. Chem. Chem. Phys.*, 2009, **11**, 3417–3423.
20. S. Damoun, G. Vande Woude, F. Mendez, and P. Geerlings, *J. Phys. Chem. A*, 1997, **101**, 886–893.
21. M. Torrent-Sucarrat, F. De Proft, P. Geerlings, and P. W. Ayers, *Chem. A Eur. J.*, 2008, **14**, 8652–60.
22. R. T. Sanderson, *Science (80-. )*, 1951, **114**, 670.
23. P. W. Ayers and R. G. Parr, *J. Chem. Phys.*, 2008, **129**, 1–7.
24. R. G. Pearson, *J. Am. Chem. Soc.*, 1963, **85**, 3533.
25. R. G. Pearson, *J. Chem. Educ.*, 1987, **64**, 561.
26. P. W. Ayers, *Faraday Discuss.*, 2007, **135**, 161.
27. R. Vuilleumier and M. Sprik, *J. Chem. Phys.*, 2001, **115**, 3454.
28. J. L. Gazquez and F. Mendez, *J. Phys. Chem.*, 1994, **98**, 4591–4593.
29. R. G. Pearson and W. E. Palke, *J. Phys. Chem.*, 1992, **96**, 3283–3285.
30. P. Hohenberg and W. Kohn, *Phys. Rev.*, 1964, **136**, B864.
31. J. L. Gazquez, *J. Phys. Chem. A*, 1997, **5639**, 9464–9469.
32. V. Tognetti, C. Morell, P. W. Ayers, L. Joubert, and H. Chermette, *Phys. Chem. Chem. Phys.*, 2013, **15**, 14465–75.
33. F. Guégan, P. Mignon, V. Tognetti, L. Joubert, and C. Morell, *Phys. Chem. Chem. Phys.*, 2014, **16**, 15558–69.
34. M. P. Mitoraj, M. Parafiniuk, M. Srebro, M. Handzlik, A. Buczek, and A. Michalak, *J. Mol. Model.*, 2011, **17**, 2337–52.
35. M. Mitoraj and A. Michalak, *J. Mol. Model.*, 2007, **13**, 347–55.
36. P. W. Ayers, J. S. M. Anderson, and L. J. Bartolotti, *Int. J. Quantum Chem.*, 2005, **101**, 520–534.
37. L.-A. Jouanno, V. Di Mascio, V. Tognetti, L. Joubert, C. Sabot, and P.-Y. Renard, *J. Org. Chem.*, 2014, **79**, 1303–19.
38. O. a Syzgantseva, V. Tognetti, A. Boulangé, P. a Peixoto, S. Leleu, X. Franck, and L. Joubert, *J. Phys. Chem. A*, 2014, **118**, 757–64.
39. R. G. Parr and W. Yang, *J. Am. Chem. Soc.*, 1984, **106**, 4049–4050.

40. N. Sablon, F. De Proft, and P. Geerlings, *J. Phys. Chem. Lett.*, 2010, **1**, 1228–1234.
41. P. Geerlings, S. Fias, Z. Boisdenghein, and F. De Proft, *Chem. Soc. Rev.*, 2014, **43**, 4989.
42. Z. Boisdenghien, S. Fias, C. Van Alsenoy, F. De Proft, and P. Geerlings, *Phys. Chem. Chem. Phys.*, 2014, **16**, 14614–24.
43. A. Michalak, M. Mitoraj, and T. Ziegler, *J. Phys. Chem. A*, 2008, **112**, 1933–9.
44. M. P. Mitoraj, A. Michalak, and T. Ziegler, *J. Chem. Theory Comput.*, 2009, **5**, 962–975.
45. P.W. Atkins and R.S. Friedmann, *Molecular Quantum Mechanics (Oxford University Press, Oxford)*, 1997.
46. G. 09, Revision D.01, M. J. Frisch, G. W. Trucks, H. B. Schlegel, G. E. Scuseria, M. A. Robb, J. R. Cheeseman, G. Scalmani, V. Barone, B. Mennucci, G. A. Petersson, H. Nakatsuji, M. Caricato, X. Li, H. P. Hratchian, A. F. Izmaylov, J. Bloino, and G. Zhe, .
47. E.J. Baerends, T. Ziegler, J. Autschbach, D. Bashford, A. Bérces, F.M. Bickelhaupt, C. Bo, P.M. Boerrigter, L. Cavallo, D.P. Chong, L. Deng, R.M. Dickson, D.E. Ellis, M. van Faassen, L. Fan, T.H. Fischer, C. Fonseca Guerra, A. Ghysels, A. Giammona, S.J.A., .
48. B. Alan and B. E. Brycki, *Chem. Soc. Rev.*, 1990, **19**, 83–105.
49. H. Chermette, I. Ciofini, F. Mariotti, and C. Daul, *J. Chem. Phys.*, 2001, **114**, 1447–1453.
50. O. Diels and K. Alder, *Justus Liebigs Ann. Chem.*, 1928, **460**, 98–122.
51. P. W. Ayers, C. Morell, F. De Proft, and P. Geerlings, *Chem. A Eur. J.*, 2007, **13**, 8240–8247.
52. P. Geerlings, P. W. Ayers, A. Toro-labbé, P. K. Chattaraj, and F. D. E. Proft, *Acc. Chem. Res.*, 2012, **45**, 683–695.
53. B. Herrera and A. Toro-Labbé, *J. Phys. Chem. A*, 2007, **111**, 5921–6.
54. A. Toro-labbé, S. Gutiérrez-oliva, J. S. Murray, and P. Politzer, *J. Mol. Model.*, 2009, **15**, 707–710.
55. A. Toro-labbe, *J. Phys. Chem. A*, 2007, **111**, 5921–5926.
56. P. Politzer, J. R. Reimers, J. S. Murray, and A. Toro-labbé, *J. Phys. Chem. Lett.*, 2010, **1**, 2858–2862.

57. F. De Proft, S. Liu, and R. G. Parr, *J. Chem. Phys.*, 1997, **107**, 3000–3006.
58. M. Torrent-Sucarrat, J. M. Luis, M. Duran, and M. Solà, *J. Mol. Struct. THEOCHEM*, 2005, **727**, 139–148.

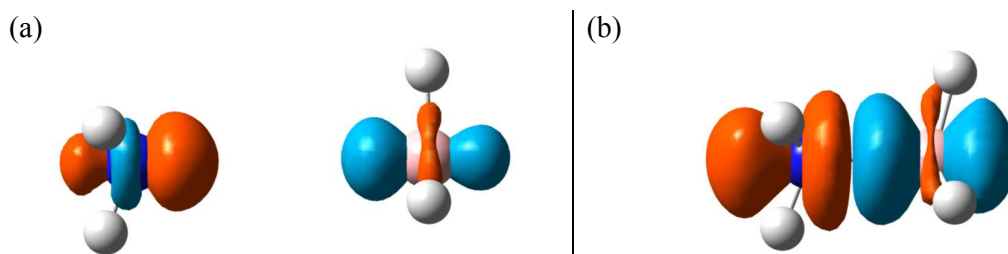


**Figure 2.**  $\text{NH}_3\text{-BH}_3$  system: (a) state specific dual descriptor for the first excited state with reactive centers separated by  $4 \text{ \AA}$  (isosurface density threshold,  $\text{IDT} = 0.015 \text{ electron/bohr}^3$ ) and (b) first NOCV pair ( $\text{IDT} = 0.003 \text{ a.u.}$ ).

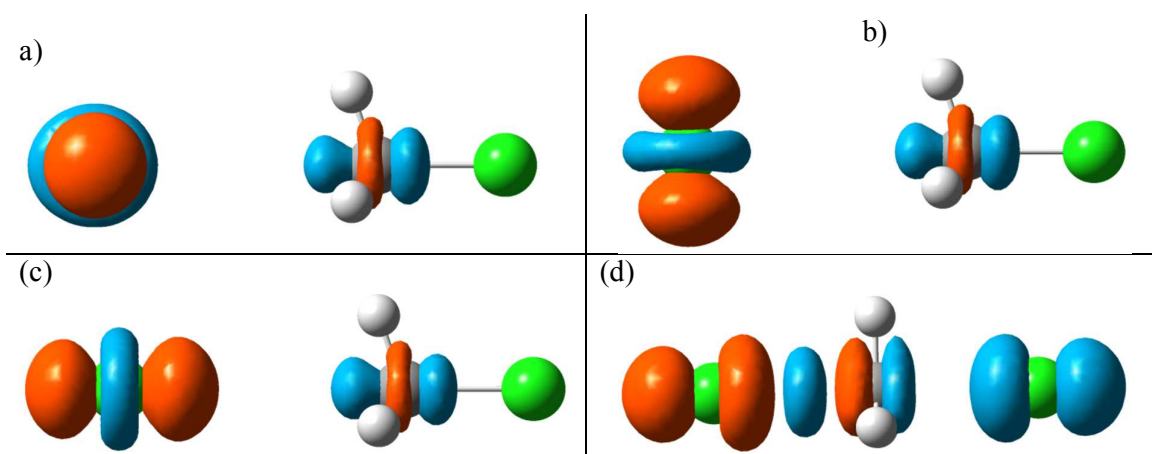


**Figure 3.**  $\text{S}_{\text{N}}2$  reaction: (a), (b) and (c) state specific dual descriptors for the first, second and third excited states respectively with reactive centers separated by  $4 \text{ \AA}$  ( $\text{IDT} = 0.009 \text{ a.u.}$ ) and (d) first NOCV pair ( $\text{IDT} = 0.004 \text{ a.u.}$ ).

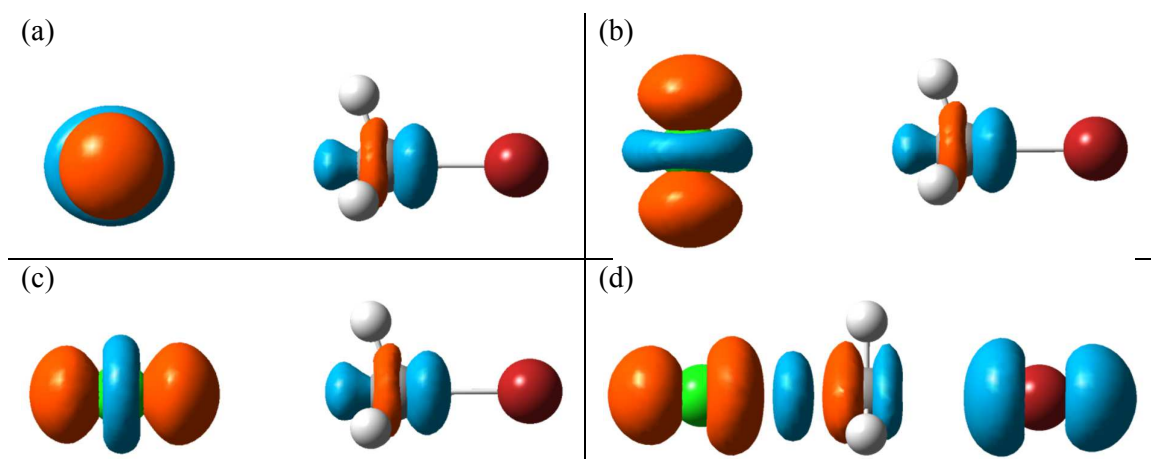


**Figure 4.** Cl<sup>-</sup>CH<sub>3</sub>-Br system: (a), (b) and (c) state specific dual descriptors for the first, second and third excited states respectively with reactive centers separated by 4 Å (IDT = 0.008 a.u.) and (d) first NOCV pair (IDT = 0.004 a.u.).

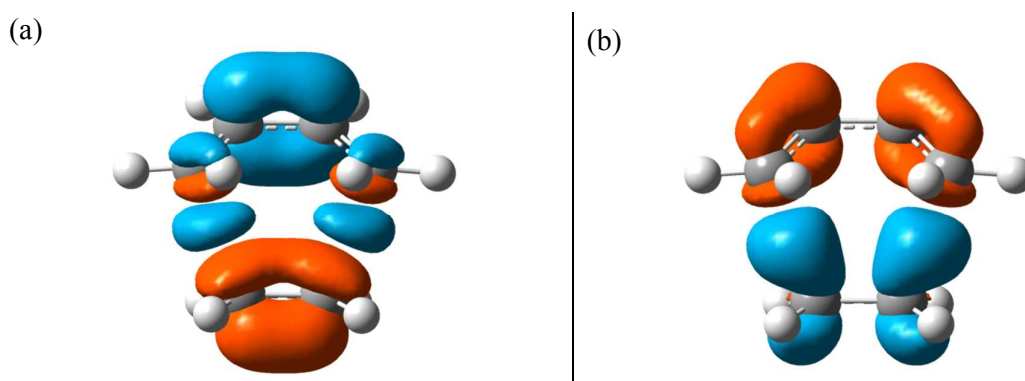


**Figure 5.** Butadiene-ethene system. (a) and (b) represent the first and second NOCV pairs respectively (IDT = 0.002 a.u.).

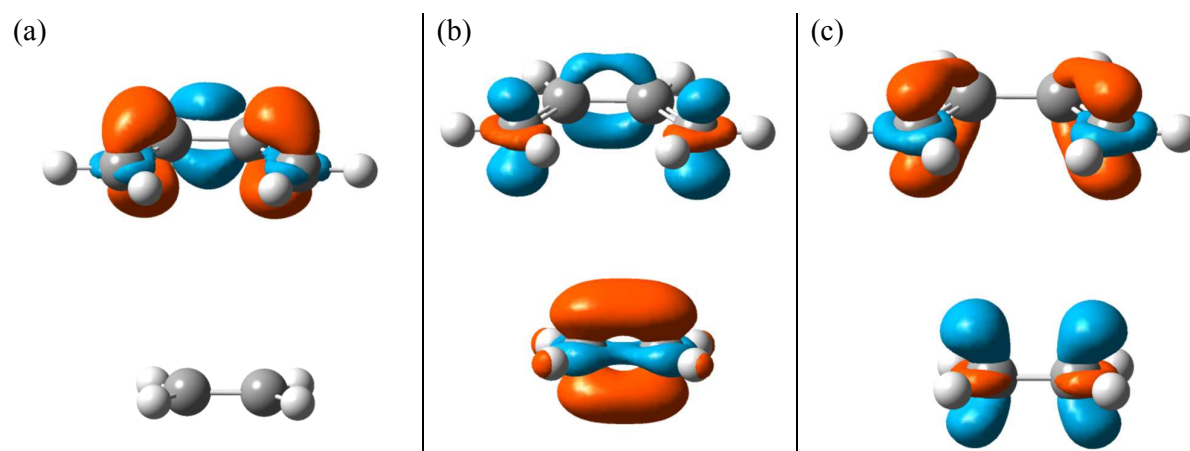


**Figure 6.** Butadiene-ethene system. (a), (b) and (c) represent the state specific dual descriptors for the first, second and third excited states respectively with reactive centers separated by 4 Å (IDT = 0.0035 a.u. for the first one and 0.0066 a.u. for the other two).

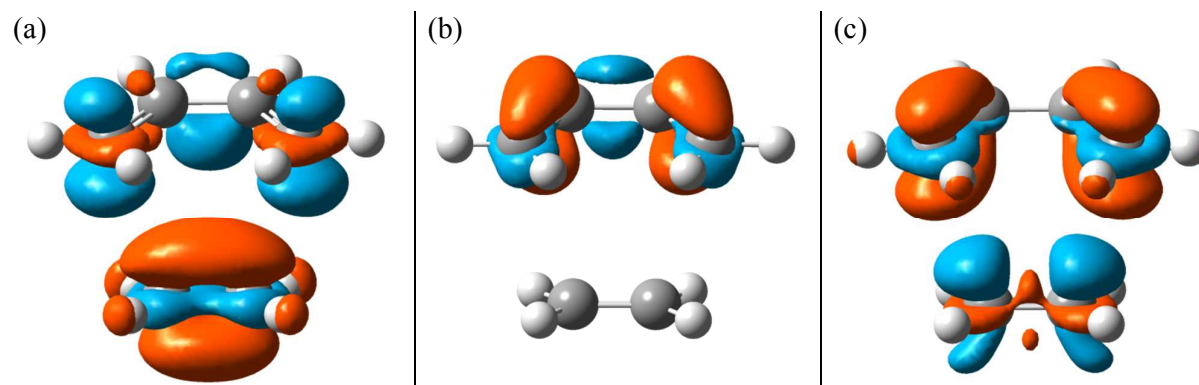


**Figure 7.** Butadiene-ethene system. (a), (b) and (c) represent the state specific dual descriptors for the first, second and fourth excited states respectively with reactive centers separated by 2.8 Å (IDT = 0.0037 a.u.).

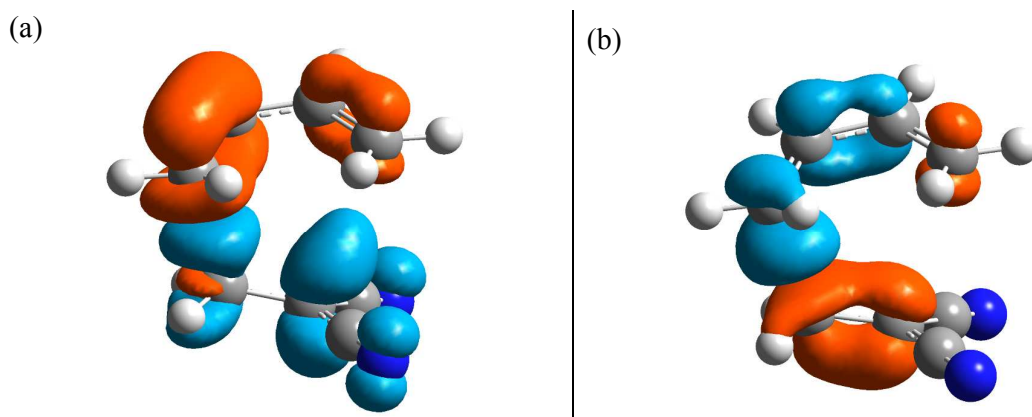


**Figure 8.** Butadiene-dicyanoethene system. (a) and (b) represent the first and second NOCV pairs respectively (IDT = 0.0022 a.u.).

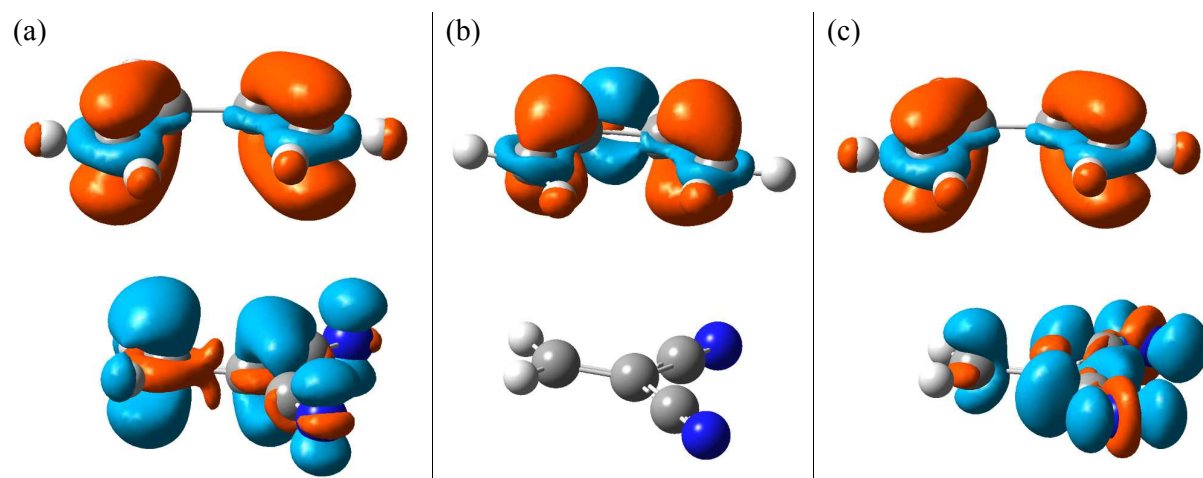


**Figure 9.** Butadiene-dicyanoethene system. (a), (b) and (c) represent the state specific dual descriptors for the first, second and third excited states respectively with reactive centers separated by 4 Å (IDT = 0.004, 0.0025 and 0.004 respectively).

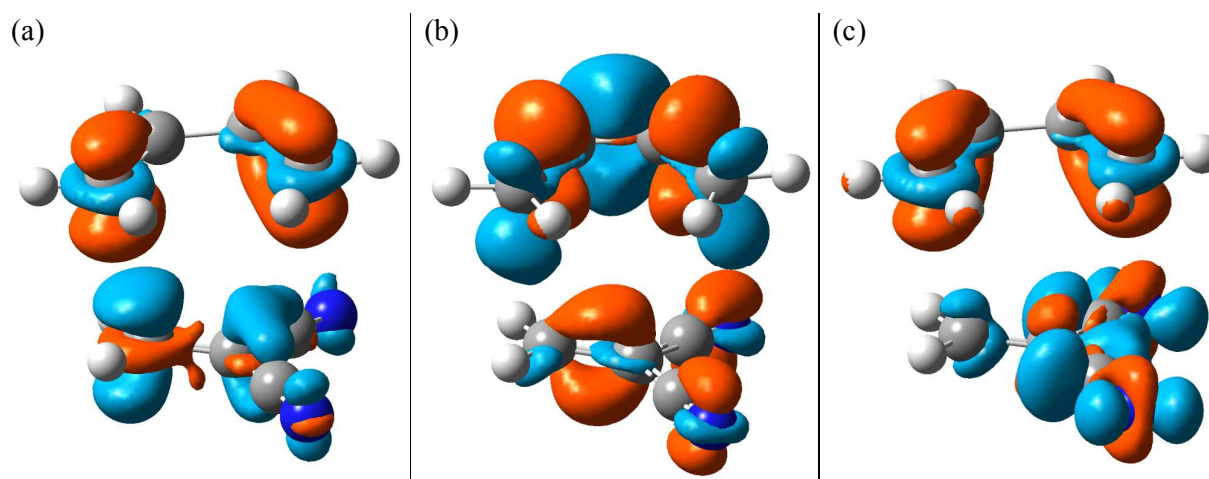


**Figure 10.** Butadiene-dicyanoethene system. (a), (b) and (c) represent the state specific dual descriptors for the first, second and third excited states respectively with reactive centers separated by 2.8 Å (IDT = 0.0037, 0.0015 and 0.0039 respectively).

SSDD		1	2	3	4
4 Å	Excitation energies (eV)	4.94	5.41	5.56	5.76
	Force constant	0.241	0.016	0.052	0.003
2.8 Å	Excitation energies (eV)	4.89	5.10	5.84	5.96
	Force constant	0.037	0.192	0	0.151

**Table 1.** Excitation energies and force constants for SSDDs of the butadiene-ethene system.

SSDD		1	2	3
4 Å	Excitation energies (eV)	3.12	4.98	5.26
	Force constant	0.027	0.147	0.005
2.8 Å	Excitation energies (eV)	3.77	4.85	5.49
	Force constant	0.155	0.045	0.002

**Table 2.** Excitation energies and force constants for SSDDs of the butadiene-dicyanoethene system.